RESEARCH PAPER

A novel passive micromixer: lamination in a planar channel system

**Terje Tofteberg · Maciej Skolimowski ·
Erik Andreassen · Oliver Geschke**

Abstract A novel passive micromixer concept is presented. The working principle is to make a controlled 90° rotation of a flow cross-section followed by a split into several channels; the flow in each of these channels is rotated a further 90° before a recombination doubles the interfacial area between the two fluids. This process is repeated until achieving the desired degree of mixing. The rotation of the flow field is obtained by patterning the channel bed with grooves. The effect of the mixers has been studied using computational fluid mechanics and prototypes have been micromilled in poly(methyl methacrylate). Confocal microscopy has been used to study the mixing. Several micromixers working on the principle of lamination have been reported in recent years. However, they require three-dimensional channel designs which can be complicated to manufacture. The main advantage with the present design is that it is relatively easy to produce using standard microfabrication techniques while at the same time obtaining good lamination between two fluids.

T. Tofteberg (✉) · E. Andreassen
SINTEF Materials and Chemistry,
PO Box 124, Blindern, 0314 Oslo, Norway
e-mail: terje.tofteberg@sintef.no

M. Skolimowski · O. Geschke
Institute for Micro- and Nanotechnology,
Technical University of Denmark,
Building 423, 2800 Kgs Lyngby, Denmark

1 Introduction

At high Reynolds numbers (typically >2400) two fluids can readily be mixed by turbulence. In microchannels with cross-sections less than one millimeter, this becomes difficult to achieve. For water at room temperature, turbulence in such a channel would require a velocity of several meters per second, which, in most cases, is unfeasible. Mixing of two fluids can still be easily done if the Peclet number is small enough. The Peclet number is defined as the ratio between advection time and diffusion time as $Pe = uL/D$, where u is the characteristic velocity, L the characteristic length and D the characteristic diffusion coefficient. When Pe is small, diffusion is fast compared to advection, meaning that mixing can usually be left to diffusion alone, e.g. as in a T-type mixer (Wong et al. 2004). This will be the case if the channels are either very small or the diffusion coefficient is very large. In the domain where the Reynolds number is small and the Peclet number is large, mixing becomes difficult. In microchannels this typically occurs if the channel dimensions are between 1 and 1,000 μm for species with low diffusivity.

There are several principles already available to achieve mixing in microchannels. Nguyen and Wu (2005) presented an overview of some of the mixers available. The coarsest classification of mixers in their article is between active and passive mixers. Active mixers can, for example, utilize pressure field disturbances (Rife et al. 2000; Niu and Lee 2003) or ultrasonic devices (Yang et al. 2001) to mix fluids. If the fluids are electrolytes, time-dependent electric or magnetic fields (Bau et al. 2001; Glasgow et al. 2004) can be used. It is also demonstrated that moving magnetic beads in a changing magnetic field can efficiently mix fluids (Suzuki and Ho 2002).

In contrast to active mixers, passive mixers are stationary and do not require any external energy input apart from the pressure drop required to drive the flow. In general, this makes passive mixers simpler to fabricate and fewer external connections are needed. In the review by Nguyen and Wu, the passive mixers for microchannels are subdivided into five categories:

(1) Chaotic advection micromixers: the channel shape is used to split, stretch, fold and break the flow. One way of achieving this is to introduce obstructions to the fluid flow in the channel (Bhagat et al. 2007; Lin et al. 2007; Hsieh and Huang 2008). Another is to introduce patterns on the channel walls that rotate the flow field, as in the staggered herringbone mixer (Stroock et al. 2002).

(2) Droplet micromixers: droplets of the fluids are generated and as droplets move an internal flow field is generated within the droplet causing a mixing of fluids. The first such mixer was demonstrated by Hosokawa et al. (1999).

(3) Injection micromixers: a solute flow is splitted into several streams and injected into a solvent flow (Voldman et al. 2000).

(4) Parallel lamination micromixers: the inlet streams of both fluids are splitted into a total of n substreams before combination. For $n = 2$, this is the classic T-type mixer. By increasing n, the diffusion length can be decreased (Bessoth et al. 1999).

(5) Serial lamination micromixers: the fluids are repeatedly splitted and recombined in horizontal and vertical planes to exponentially increase their interfacial area. One well-known example is the Caterpillar mixer (Schönfeld et al. 2004) but other similar designs have also been proposed (Cha et al. 2006; Xia et al. 2006).

In this report we present a lamination mixer that is similar to the serial lamination mixers. However, whereas both the parallel and the serial lamination mixers described in the literature need out of plane channels to split and rejoin the streams, our mixer has all channels in one plane. This means that the mixer can be fabricated by just bonding a planar lid on the top of a structured channel. On the other hand, a three-dimensional channel will need at least two structured parts which have to be aligned precisely in the fabrication process. Thus, the main advantage of the present mixer when compared with active mixers and other lamination mixers is the ease of fabrication. The structures can easily be mass produced using polymer replication techniques such as injection molding or hot embossing.

To the authors knowledge this is the first time a mixer working on the principle of splitting and recombining in such a simple design is presented. In order to achieve the
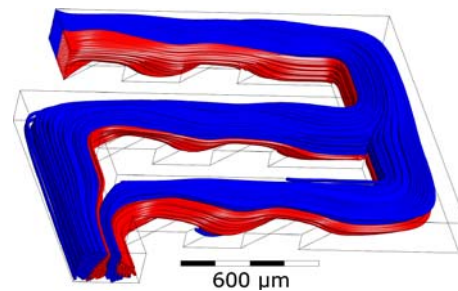

Fig. 1 Simulated flow field in one mixing module showing lamination in the Stokes flow regime ($Re < 5$). The two fluids enter in the *upper left* corner. The interfacial area between the two has approximately tripled at the exit in the *lower left* corner

folding, the flows are rotated 90° between each splitting and rejoining. This helical flow pattern is achieved by patterning the channel bed. An illustration of a mixing module of this kind is shown in Fig. 1. In this figure, the simulated streamlines are colored according to their origin.

The present mixer has been realized using several microfabrication techniques.

- Direct laser ablation of channels and grooves in poly(methyl methacrylate) (PMMA).
- Direct micromilling in polycarbonate (PC) and PMMA.
- Milling of the negative structure in aluminum and replication with injection molding in polystyrene (PS).
- Milling of the negative structure in PMMA and replication in polydimethylsiloxane (PDMS).

The results presented in this article relate to mixers milled directly in PMMA. We want to emphasize that the design, because of its open structure and lack of intricate details, can easily be realized using a range of microfabrication techniques.

2 Procedure

2.1 Microfabrication

As a main fabrication method micromilling (Mini-Mill/3PRO, Minitech Machinery Corp., USA) in PMMA (Röhm GmbH & Co. KG, Germany) was used. First, channels with depth of 50 μm and width of 300 μm (equal to the diameter of the tool) were milled. In the bed of the channels 200 μm wide grooves were fabricated using a ⌀100 μm milling tool. This tool diameter was chosen to minimize the fillet radius on the corners of the grooves. Cut feed speed was 70 mm/min and spindle rotation was 4,000 RPM.

As an alternative fabrication method, laser ablation (48-5S Duo Lase carbon dioxide laser, SYNRAD Inc., USA) was used. The channels were obtained using a 10 W laser beam (wavelength 10.6 μm) and a focusing lens with

200 mm focal length (beam diameter 290 μm). The ablation velocity was adjusted to 300 mm/min. For ablation of 200 μm grooves, an 80 mm focal length lens was used (beam diameter 90 μm) and the power was reduced to 4 W. Ablated structures had a Gaussian-like cross-section as reported earlier (Klank et al. 2002).

The microdevice was sealed with a lid using a silicone adhesive thin film (ARcare® 91005, Adhesive Research Ireland Ltd.). Thermal bonding and laser bonding methods also gave good results.

2.2 Confocal laser scanning microscopy measurements

To investigate the performance of the designed micromixer two dyes were used: Rhodamine B and Fluorescein. The dyes were dissolved in phosphate buffered saline (pH 7.4) with 0.2% sodium dodecyl sulfate (SDS) (all from Sigma-Aldrich, Denmark A/S). Confocal laser scanning microscopy (Zeiss LSM 510 Meta, Brock og Michelsen A/S, Denmark) was done using a 40× Fluar oil immersion objective. A 488 nm Argon laser was used for exciting Fluorescein and a 543 nm HeNe laser for Rhodamine B. The pinhole was adjusted for approximately 5 μm z axis slice thicknesses. The solutions were pumped through the microdevice by a syringe pump (model 540060, TSE Systems GmbH, Germany) with flow-rate according to the desired Reynolds number.

2.3 Simulations

The mixing efficiency was investigated using 3D finite volume simulations in ANSYS CFX 11.0. The procedure adopted is similar to the one described by Mendels et al. (2008) where the fluids are treated as isothermal and incompressible Newtonian fluids following the Navier–Stokes equations.

$$\nabla \cdot \mathbf{u} = 0 \tag{1}$$

$$\rho \left[\frac{\partial \mathbf{u}}{\partial t} + \mathbf{u} \cdot \nabla \mathbf{u} \right] = -\nabla p + \eta \nabla^2 \mathbf{u} \tag{2}$$

Here $\mathbf{u}$ is the velocity vector, ρ the density, η the viscosity and t the time. To track the location of the interface between the two fluids an additional concentration variable c is transported through the domain by convection and diffusion.

$$\frac{\partial c}{\partial t} + \mathbf{u} \cdot \nabla c = D \nabla^2 c \tag{3}$$

Since the mixer works by lamination, the efficiency of the mixer was best evaluated in the absence of diffusion, therefore the diffusion coefficient, D, was set to 0 in the simulations.

At the inlet, a sharp step in c is prescribed, representing two completely separated fluids. Because of numerical diffusion, it is necessary to have a fine mesh at the interface between the two phases. This interface is not initially known and in order to define a fine mesh here, an adaptive meshing procedure was used. Equations 1–3 were first solved on a relatively coarse mesh. When convergence was obtained, the mesh was refined where the variation in c over an element edge exceeded a given value. This procedure was repeated six times with an increasingly finer mesh, until convergence in mesh size. The fluid properties in the simulations are the same as water at 20°C with $\eta = 1.002$ mPa s and $\rho = 998$ kg/m^3.

2.4 Validation

To validate the simulations, a channel was made using laser ablation. The channel has a cross-section of 300 μm × 50 μm, and 50 μm deep, 200 μm wide grooves inclined 55° relative to the channel axis. The shape of the grooves was measured using confocal microscopy and the measured geometry was used as a basis for simulations. The resulting rotation can be seen in Fig. 2. It can be seen that there is a good qualitative agreement between the simulated and measured rotations. Using this geometry, the closest thing to a 90° rotation occurs after three grooves. It can also be seen that after six grooves, a full 180° rotation is observed in the simulations. The experimental data indicates that this rotation is taking place already after five grooves. Note also the almost perfect match between the cross-section after the first and seventh grooves in the simulations, which is also seen after the first and sixth grooves in the experiments.

2.5 Design optimization

As can be seen in Fig. 2, the rotation after three grooves is not exactly a straight angle. There is also some deformation of the interface between the two tracers; it is no longer a straight line as was the case at the inlet. Three design parameters were varied in a full factorial design to see how a 90° rotation could best be achieved:

- the groove angle (45°–55°–65°),
- the depth of the grooves (50–100–200 μm),
- the depth of the channel (50–100–200 μm).

The channel width was fixed to 300 μm. The design optimization was performed using simulations in CFX of straight channels to find the configuration that gave a rotation of the flow as close to 90° as possible. The best results were obtained with a groove angle of 55°, a channel depth of 50 μm and a groove depth of 50 μm which are the parameters used in the following experiments. This optimal
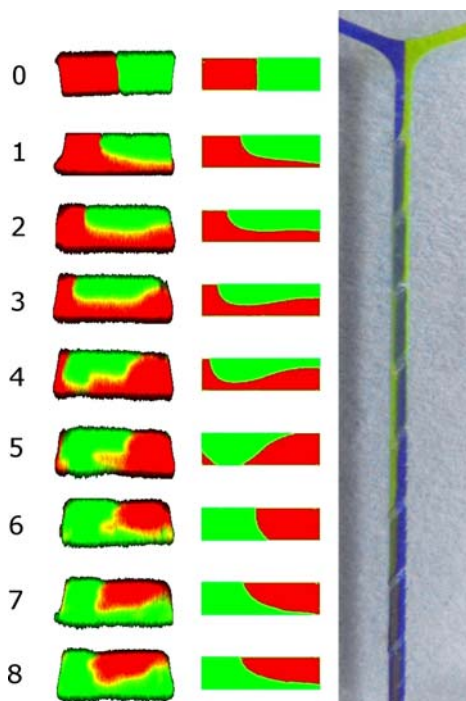
Fig. 2 Helical rotation of the flow field in a straight channel with grooves on the channel bed in the Stokes flow regime ($Re \sim 1$). *Left* confocal fluorescence microscopy measurements of the distribution of rhodamine (*red, left at the inlet*) and Fluorescein (*green, right at the inlet*). *Center* simulated flow field. *Right* photography showing a top view of channel. The *numbers* indicate the cross-section after a given number of grooves, which can be seen in the *right* image

design is shown with dimensions in Fig. 3. Note that this is not a global optimum but only the optimum within the limited space sampled. Other authors have studied the optimization of helical flow patterns by patterning the channel (Yang et al. 2005, 2008) and it is likely that further optimization of the structure is possible.
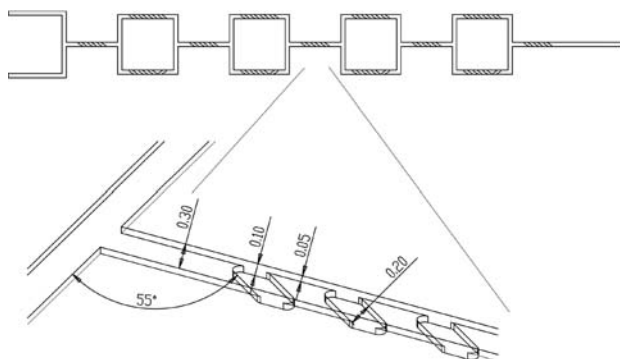

Fig. 3 Design showing four mixing modules (*above*). Detailed view of the grooves with dimensions indicated (in mm) (*below*). The main channel is 50 μm × 300 μm with 50 μm deep, 200 μm wide grooves, inclined 55° relative to the channel axis

3 Results and discussion

The lamination observed experimentally and in simulations, for one module, is shown in Fig. 4. There is a good agreement between the simulated and measured rotations of the flow field. It is also demonstrated that the mixer is able to laminate the flow field as desired.

The lamination, as measured with confocal microscopy, after one to four modules is shown in Fig. 5a. Note that after three modules the two fluids are mixed well. The different laminae can still be seen, demonstrating that it is the stretching and folding effect of the device that is mixing the fluids. The mixing efficiency will in general be dependent on the Peclet number, showing better mixing at lower Peclet numbers. The diffusion coefficients for Rhodamine B and Fluorescein alone in water are 3.6×10^{-10} and 4.9×10^{-10} m^2/s, respectively (Rani et al. 2005). Note that Rhodamine B is hydrophobic and is likely to form micelles with sodium dodecyl sulfate, increasing the diffusion coefficient. This increased diffusion coefficient was not measured. The Peclet number for Fluorescein in the setup shown in Fig. 5 is 9700. The effective Peclet number for Rhodamine B is probably larger than for Fluorescein because of the micelles. This is indicated by the fact that the evaluated degree of mixing for Rhodamine B rises slower than for Fluorescein as can be seen in Fig. 5c.

In the original staggered herringbone article by Stroock et al. (2002), the efficiency is evaluated by measuring the standard deviation σ in fluorescence at different locations. The distance required to achieve a reduction in standard
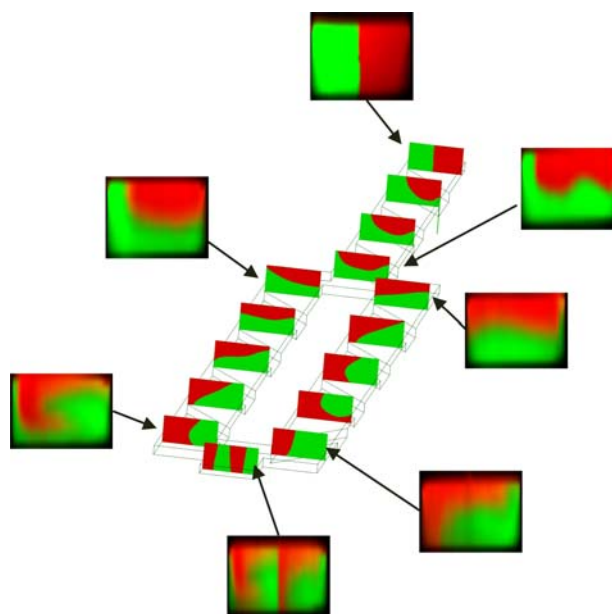

Fig. 4 Concentration distributions within one mixing module. The images on the geometry show the simulated distribution and the outer ones are confocal microscopy measurements

Fig. 5 a Confocal microscopy images showing planes at $z = h/2$, where h is the channel depth. The images show from the top the intensity at the entrance and after one to four full modules ($Re = 5$). The modules can be seen in Fig. 3. **b** Normalized intensity of the two fluorophores measured across the cross-sections in **a**. **c** The index of mixing evaluated using the variance in the data from **b**. **d** The standard deviation of the intensities from **b** including a line showing the criteria used for mixing
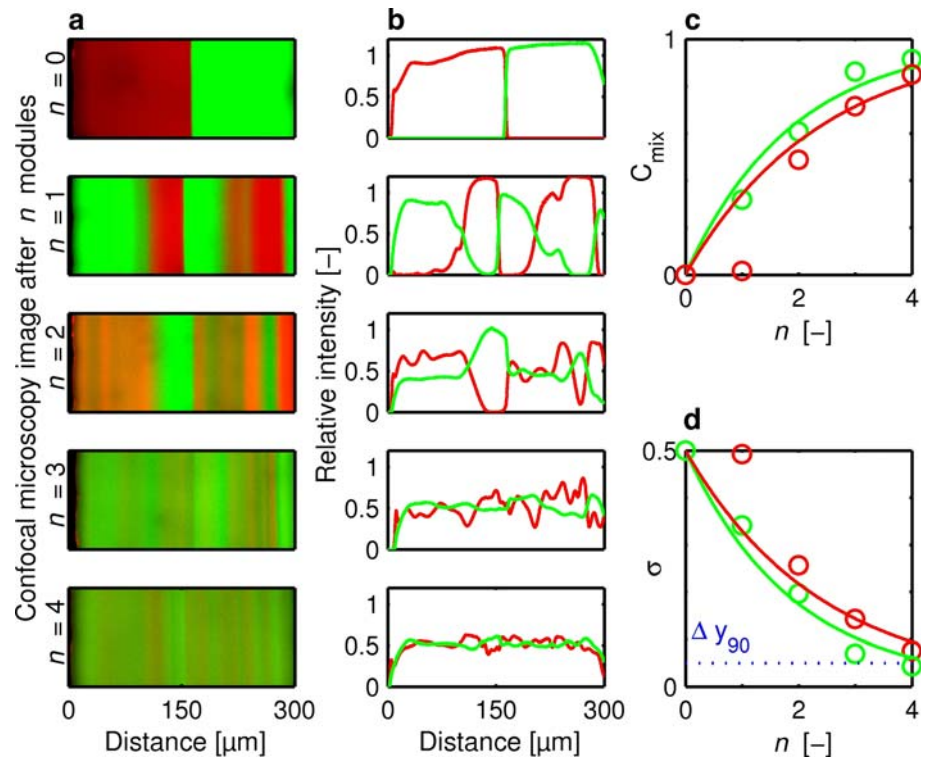
deviation by 90% relative to the inlet, Δy_{90}, is taken as an indication of the length of mixer required. This standard deviation for the present mixer is seen in Fig. 3d after one to four full modules and it can be seen that this criterion has been met for the fluorophore with the highest diffusivity, Fluorescein, after four modules. The larger, and slower diffusing rhodamine B is close to achieving this criterion. In Stroock et al. this criterion is met after between 3.5 ($Pe = 2000$) and 8.5 ($Pe = 2 \times 10^5$) rotation cycles. Note that the standard deviation measure for mixing will be dependent on the resolution of the confocal microscopy used and therefore these values for mixing efficiency are not directly comparable from study to study. They are still included here for an indication of the mixing efficiency.

To quantitatively evaluate the mixing efficiency, we define the index of mixing as in (Liu et al. 2004) as

$$C_{mix} = \frac{\sigma_{inlet} - \sigma}{\sigma_{inlet}} \tag{4}$$

where σ is the standard deviation of the fluorescence intensity. They use simulation to evaluate the mixers and sigma is the standard deviation in the concentration of a phase variable. They find that the index of mixing for the herringbone mixer when mixing solutions of glycerol and water is approximately 0.5 ($Pe = 1000$) after two full mixing cycles. The mixing index for the present mixer is shown in Fig. 5c.

3.1 Reynolds number dependence

The simulated lamination for two different Reynolds numbers is shown in Fig. 6. Up to a Reynolds number of 5 (flow rate 50 µl/min), changing the flow rate does not change the lamination process. The characteristic length, is in this case, taken as the hydraulic diameter of the channel (85 µm) and the characteristic velocity is the volume flow divided by the channel cross-section (300 µm × 50 µm) where no grooves are present. It can be seen that in the Stokes flow regime, almost perfect lamination is observed. As the momentum effects become more important,
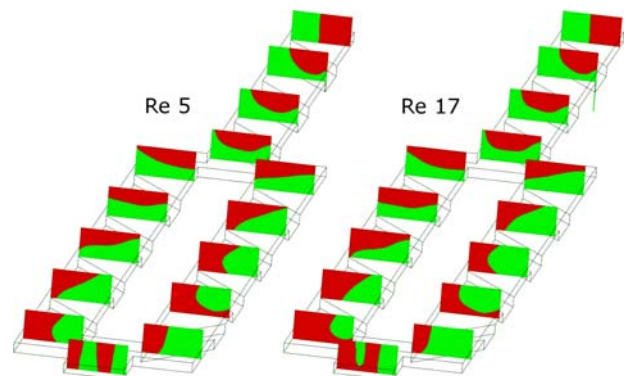

Fig. 6 Simulated lamination as a function of the Reynolds number. For $Re < 5$, the profiles are independent of Re to the accuracy of this graphical representation

however, the helical rotation of the flow field changes. The structure still works as a mixer, but since the helical rotation outside the Stokes flow regime is Reynolds number dependent, it is not given that the two substreams join each other after the designed 90° rotation for Reynolds number above five. For the staggered herringbone mixers, which also reliy on grooves on the channel bed to rotate the flow field, it has been reported that at high Reynolds numbers (>10) vortices form in the grooves which significantly reduce the rotation (Williams et al. 2008). Similar effects are also seen for three-dimensional mixers working on the split and recombine principle, for example, good lamination is only observed with the caterpillar mixers for low Reynolds numbers (<30, Schönfeld et al. 2004).

3.2 Stacking of design

In this report, the focus has not been on making the design as compact as possible. This can, however, be done when considering the layout in Fig. 1. By changing the direction of flow after each rotation of the flow field the overall shape of one mixer module is rectangular. The module shown measures 1.5×1.7 mm and the rectangular overall shape makes it easy to pack it densely on a chip device.

4 Conclusions

A new concept for a passive micromixer has been developed. It is shown that the combination of patterning the channel bed and splitting and recombining the streams can be used to make controlled lamination in a 2D channel system. This is shown using both numerical simulations and experiments with prototypes. The design can easily be realized using a range of microfabrication techniques and mass produced using, for example, injection molding.

In the design optimization used in this work only a small subset of the design parameter space was investigated. A further optimization of the design with respect to mixing efficiency on an area as small as possible should be carried out in the future. It is also possible to change the mixer to divide the flow into more than two substreams. Preliminary studies indicate that splitting into three or four substreams can be used to obtain better mixing on a smaller area. Further examination of this question should be made in the future.

References

Bau HH, Zhong J, Yi M (2001) A minute magneto hydro dynamic (MHD) mixer. Sens Actuat B Chem 79:207–215

Bessoth FG, de Mello AJ, Manz A (1999) Microstructure for efficient continuous flow mixing. Anal Commun 36:213–215

Bhagat AAS, Peterson ETK, Papautsky I (2007) A passive planar micromixer with obstructions for mixing at low Reynolds numbers. J Micromech Microeng 17:1017–1024

Cha J, Kim J, Ryu SK, Park J, Jeong Y, Park S, Park S, Kim HC, Chun K (2006) A highly efficient 3D micromixer using soft PDMS bonding. J Micromech Microeng 16:1778–1782

Glasgow I, Batton J, Aubry N (2004) Electroosmotic mixing in microchannels. Lab Chip 4:558–562

Hosokawa K, Fujii T, Endo I (1999) Droplet-based nano/picoliter mixer using hydrophobic microcapillary vent. In: 12th IEEE international conference on micro electro mechanical systems (MEMS 99), pp 388–393

Hsieh S-S, Huang Y-C (2008) Passive mixing in micro-channels with geometric variations through μPIV and μLIF measurements. J Micromech Microeng 18:065017

Klank H, Kutter JP, Geschke O (2002) CO2-laser micromachining and back-end processing for rapid production of PMMA-based microfluidic systems. Lab Chip 2:242–246

Lin Y-C, Chung Y-C, Wu C-Y (2007) Mixing enhancement of the passive microfluidic mixer with J-shaped baffles in the tee channel. Biomed Microdevices 9:215–221

Liu YZ, Kim BJ, Sung HJ (2004) Two-fluid mixing in a microchannel. Int J Heat Fluid Flow 25:986–995

Mendels DA, Graham EM, Magennis SW, Jones AC, Mendels F (2008) Quantitative comparison of thermal and solutal transport in a T-mixer by FLIM and CFD. Microfluid Nanofluid 5:603–617

Nguyen NT, Wu ZG (2005) Micromixers—a review. J Micromech Microeng 15:R1–R16

Niu X, Lee YK (2003) Efficient spatial–temporal chaotic mixing in microchannels. J Micromech Microeng 13:454–462

Rani SA, Pitts B, Stewart PS (2005) Rapid diffusion of fluorescent tracers into Staphylococcus epidermidis biofilms visualized by time lapse microscopy. Antimicrob Agents Chemother 49:728–732

Rife JC, Bell MI, Horwitz JS, Kabler MN, Auyeung RCY, Kim WJ (2000) Miniature valveless ultrasonic pumps and mixers. Sens Actuat A Phys 86:135–140

Schönfeld F, Hessel V, Hofmann C (2004) An optimised split-and-recombine micro-mixer with uniform 'chaotic' mixing. Lab Chip 4:65–69

Stroock AD, Dertinger SKW, Ajdari A, Mezic I, Stone HA, Whitesides GM (2002) Chaotic mixer for microchannels. Science 295:647–651

Suzuki H, Ho CM (2002) A magnetic force driven chaotic micromixer. In: 15th IEEE international conference on micro electro mechanical systems (MEMS 2002), pp 40–43

Voldman J, Gray ML, Schmidt MA (2000) An integrated liquid mixer/valve. J Microelectromech Syst 9:295–302

Williams MS, Longmuir KJ, Yager P (2008) A practical guide to the staggered herringbone mixer. Lab Chip 8:1121–1129

Wong SH, Ward MCL, Wharton CW (2004) Micro T-mixer as a rapid mixing micromixer. Sens Actuat B Chem 100:359–379

Xia HM, Shu C, Wan SYM, Chew YT (2006) Influence of the Reynolds number on chaotic mixing in a spatially periodic

micromixer and its characterization using dynamical system techniques. J Micromech Microeng 16:53–61

Yang Z, Matsumoto S, Goto H, Matsumoto M, Maeda R (2001) Ultrasonic micromixer for microfluidic systems. Sens Actuat A Phys 93:266–272

Yang JT, Huang KJ, Lin YC (2005) Geometric effects on fluid mixing in passive grooved micromixers. Lab Chip 5:1140–1147

Yang JT, Fang WF, Tung KY (2008) Fluids mixing in devices with connected-groove channels. Chem Eng Sci 63:1871–1881